Tunable Spectral Ordering and Directional Radiation in Magnetic Plasmon Oligomers

Nicholas P. Montoni, Steven C. Quillin, Charles Cherqui, and David J. Maisello*

Department of Chemistry, University of Washington, Seattle, WA 98195

E-mail: masiello@chem.washington.edu

Abstract

Magnetic plasmon resonances, the collective response of cyclic arrangements of plasmonic nanoparticles, have been of great recent interest due to their ability to couple to both the electric and magnetic field of light. At small sizes, these metal nanoparticle aggregates, called magnetic oligomers, satisfy the quasistatic approximation and couple weakly to the magnetic field of light. At large sizes, the magnetic and electric effects interfere with one another, resulting in size- and frequency-dependent radiative properties. This allows for unprecedented control over the directionality of light scattered from these systems, opening the path to applications that require direct control over the directionality of specific colors of light.

Keywords

plasmon, hybridization, magnetic, retardation

1 Introduction

Interest in the collective magnetic response of arrays of metal nanoparticles, called magnetic plasmon resonances, has exploded in recent years. This is due to the possibility of applying magnetic plasmon resonances to problems such as biological sensing and imaging, electromagnetic cloaking, and information processing.[1–11] A magnetic plasmon is the closed-loop collective plasmonic resonance of a ring-like arrangement of metal nanoparticles, called a plasmonic oligomer. The properties of single oligomers have been well-documented, as well as the properties of infinite metal nanoparticle arrays, but there are open questions regarding the behavior of few-oligomer systems.[12–17] Problems such as magnetic plasmon hybridization and electric-magnetic plasmon interference are still unsolved and are the key to utilizing the unique optical properties of magnetic oligomers.

There is also some ambiguity in how to model magnetic plasmonic systems in the few-oligomer size regime. For single oligomers or small arrays of nanoparticles, the quasistatic approximation is a good approach. This assumes that a system is so small that light propagates accross it infinitely quickly, meaning that only electric near-field effects matter. One such work employing this approach describes one-, two-, and six-oligomer systems using both a quasistatic tight-binding model and full-wave simulations.[16] In this way the model differs from the simulations, which keep the speed of light finite and incorporate all retaradtion effects.[18] Between this model and the simulations arose a discrepancy: in the spectral ordering of the closed-loop magnetic modes, the tight-binding model predicts that the magnetic modes with the most nodes (the most changes in magnetic field polarity) should be lower in energy while simulations predict that the magnetic modes with no nodes should be lower in energy. Considering that magnetism is a result of a finite speed of light, and therefore is entirely the result of retardation, it is understandable that for large, multi-oligomer systems that store energy in the magnetic field the quasistatic approximation should break down.

In the single-oligomer regime, the quasistatic approximation is good and describes magnetic oligomers accurately.[13,19] While retardation effects have been considered in studies

of both large MNPs and infinite MNP arrays,[20–28] the breakdown of the quasistatic approximation and size-dependent tunability have not been studied in magnetic oligomers. Incorporating retardation effects into a simple model, such as the tight-binding model previously mentioned,[16] is the first step to accurately modeling magnetic plasmon-supporting aggregates. This model not only explains the reason why a quasistatic model and full-wave simulations should disagree, but it shows in addition that the magnetic modes of planar, few-oligomer systems exhibit dynamic and tunable energy-ordering. As suggested by previous work, single magnetic oligomers exhibit electric-magnetic interferences.[12] Planar, multi-oligomer systems exhibit similar properties with both size- and frequency-dependence. As a result, it is possible to use magnetic oligomers to scatter light of specific colors in different directions, suggesting unprecedented tunability and control of light.

2 Model Systems and Magnetic Plasmon Resonances

This work begins by preparing three model systems for study, all composed of identical silver spheres of radius r_0 and built in analogy to conjugated hydrocarbon rings (see Figure 1): a system of ten particles arranged like the carbon atoms in naphthalene (the 2-mer), a system of fourteen particles resembling anthracene (the linear 3-mer), and a system of thirteen particles arranged like phenalene (the triangular 3-mer). Mapping the dipole plasmon on each particle to a harmonic oscillator and giving each oscillator two degrees of freedom in the plane of the oligomer results in an equation of motion for each dipole[29]

$$\ddot{\mathbf{q}}_i = -\omega_{\mathrm{sp}}^2 \mathbf{q}_i + \frac{e}{m_{\mathrm{sp}}} \sum_{j \neq i} \mathbf{E}_j(\mathbf{r}_i) \tag{1}$$

where ω_{sp} is the natural frequency of a single electric plasmon, $m_{\mathrm{sp}} = e^2/\alpha_{\mathrm{sp}}\omega_{\mathrm{sp}}^2$ is the surface plasmon effective mass defined by the polarizability α_{sp}, the plasmon oscillator dipole moment $\mathbf{d}_i = e\mathbf{q}_i$, and $\mathbf{E}_j(\mathbf{r}_i)$ is the fully retarded electric field from the j^{th} dipole at the position of the i^{th} dipole and is defined as

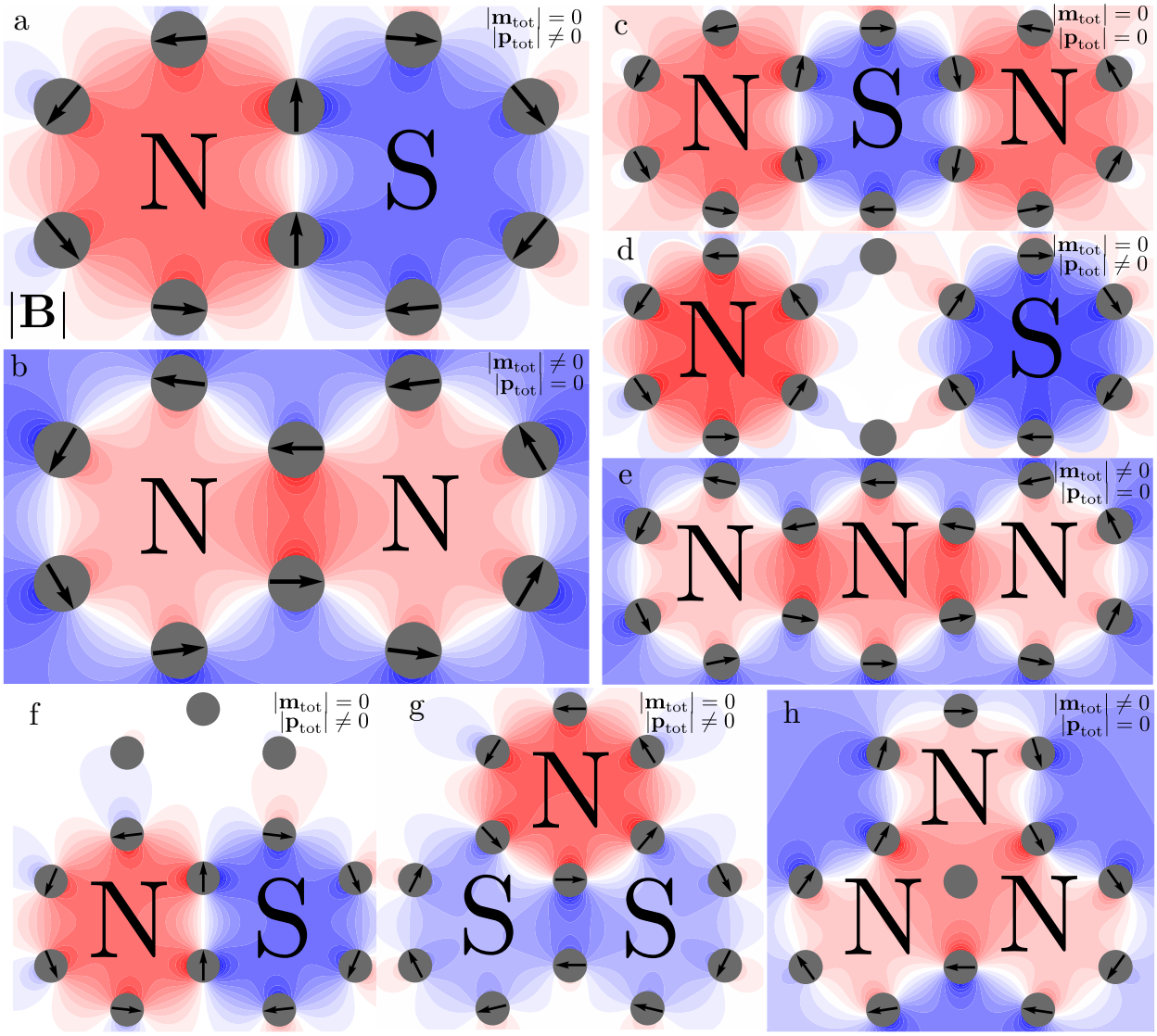

Figure 1: Magnetic field plots of the two-ring (a and b), linear three-ring (c, d, and e), and triangular three-ring (f, g, and h) oligomers. Each system supports a number of closed-loop magnetic plasmon resonances equal to the number of rings in the system. The nodeless magnetic plasmons (b, e, and h) support a net magnetic dipole moment and are excitable by the magnetic field of light. The single-node magnetic plasmons (a, c, f, and g) support net electric dipole moments. The two-node magnetic mode of the linear three-ring system is inaccessible by light.

$$\mathbf{E}_j(\mathbf{r}_i) = \mathbf{\Lambda}_{ij} \cdot \mathbf{d}_j = \left\{ \left(\frac{1}{r_{ij}^3} - \frac{ik}{r_{ij}^2} \right) (3\hat{\mathbf{n}}_{ij}\hat{\mathbf{n}}_{ij} - \mathbf{1}) + \frac{k^2}{r_{ij}} (\mathbf{1} - \hat{\mathbf{n}}_{ij}\hat{\mathbf{n}}_{ij}) \right\} \frac{e^{\mathrm{i}kr_{ij}}}{\varepsilon_b} \cdot \mathbf{d}_j. \qquad (2)$$

Here, $\hat{\mathbf{n}}_{ij}$ is the unit vector connecting two dipoles separated by distance r_{ij}, $k = \sqrt{\varepsilon_b}\omega/c$ is the wavenumber of the collective mode with frequency ω, and ε_b is the dielectric constant of the background medium. Using just the fully retarded electric field, we have incorporated all necessary retardation effects.[18]

Solving the system of Equations 1 for all of the dipoles in a single aggregate yields a set of hybridized modes equal to the number of degrees of freedom, in this case, two times the number of particles. However, each system supports a number of closed-loop magnetic plasmons equal to the number of nanoparticle rings. The eigenvectors of these collective modes represent the dipole moments on each nanoparticle. Figure 1 shows these magnetic mode eigenvectors overlayed with plots of the signed magnetic field magnitude of each normal mode. Each mode is named for its particular magnetic field distribution after the poles of a magnet (e.g. the 2-mer's North-South and North-North mode). It is important to note which magnetic modes can couple to the far-field. The top right-hand corner of each field plot in Figure 1 displays whether the magnetic mode depicted exhibits a net electric dipole, a net magnetic dipole, or neither. Because it is possible to excite both a magnetic dipole moment and an electric dipole moment orthogonal to one another in these oligomers, they exhibit tunable directionality in the light that they scatter. This will be an important discussion later in this work when outlining the properties of magnetic oligomer systems. To begin, we apply the fully retarded tight-binding model to the magnetic modes of the 2mer system to determine where and why the quasistatic approximation breaks down in magnetic oligomer systems.

3 Spectral Ordering of Magnetic Modes in the 2-mer

To determine the breakdown of the quasistatic limit as a function of size and the impact of incorporating retardation effects, we introduce two parameters: scale and spacing. Defining a nearest-neighbor distance between individual nanoparticles $r_{\mathrm{nn}} = (s+2)r_0$ allows both scale (changing r_0 with fixed s) and spacing (changing s withfixed r_0) to be vary independently. Figure 2 shows the results of varying both r_0 (a-d) and s (e-h) in vacuum and in water ($\varepsilon_b = 1.77$). At small sizes the magnetic modes preserve the quasistatic ordering predicted in previous work, which is to be expected when the oligomer system fits easily into a wavelength of light and the near-field dominates the electric field.[16] As the system scale increases, the magnetic modes change order. This is due to the far-field term in the electric field becoming significant in magnitude, as shown inFIgure 2b. In other words, as the system gets larger, the near-field interaction becomes less important relative to other parts of the electric field. At even larger sizes, the modes switch again. The second switch is unexpected and possibly counterintuitive, as the modes recover the spectral ordering predicted in the quasistatic limit. However, this does not mean that the quasistatic approximation is suddenly accurate again for these larger systems. Rather, both switches are due entirely to retardation effects. Looking at the interaction energies of each mode,

$$U_{\mathrm{int}} = -\sum_i \mathbf{d}_i \cdot \sum_{j \neq i} \mathbf{E}_j(\mathbf{r}_i), \tag{3}$$

with $\mathbf{E}_j$ defined through Equation 2, the introduction of more terms to the electric field is the cause of the mode switching. The third term of Equation 2, the far-field, carries the opposite sign of the near- and intermediate-field terms, leading to opposite splitting. The splitting between the modes in the near- and intermediate-field has the same sign, so each contributes a shift in the same direction. Combining this with the opposite splitting in the far-field results in mode switching at values of r_0 where the sum of all of the splittings is zero. Perhaps more interestingly, in water the crossing points are shifted towards smaller scale. This is

to be expected, as the wavelength of light is compressed in a medium, meaning that light sees objects as much bigger than they really are. This analysis shows that the quasistatic approximation is good for very small magnetic oligomers in vacuum, and for smaller still oligomers in medium. This can also be explained through the impact of a dielectric medium on coupling strength. While a medium should contribute an overall increase to the coupling strength (which is predicted in Figure 2b and f), the far-field term should be more drastically impacted due to its extra ε_b-dependence through its k^2 term.[30] Through comparison with simulation (dashed lines in Figure 2a), it can be shown that this simple and efficient model is accurate to within 0.05 eV and accurately describes the behavior of magnetic plasmon oligomers.

While good for theoretical studies of system properties, scale is not tunable in real time, meaning these properties can't be easily measured. Recent research has focused heavily on finding controllable and reversible ways to manipulate the aggregation scheme of a metal nanoparticle array using tools like DNA, polymers, and stretchable embedding media.[31–34] We employ this idea by fixing the particle radii and the aggregation scheme of the structure and inflating the interparticle distances. Figure 2e-h shows the results of fixing r_0 at 15 and 30 nm and increasing s. Increasing the distance between particles regardless of particle size and environment weakens the coupling as the distance approaches infinity, which can be seen in Equation **??**. As a result, the collective frequencies of the magnetic modes approach the single plasmon frequency. On the way, the modes oscillate about each other, exhibiting multiple crossings. The amplitude of these crossings appears to increase with increasing particle size and with increasing background dielectric constant, which can be seen in Figure 2f and h. The quasistatic approximation cannot explain this phenomenon. The fully retarded electric field contains a complex exponential term that depends on interparticle separation. It is this term that dresses all of the interaction terms in the field and changes the sign of the interaction from negative to positive at certain distances. This is clear evidence that the magnetic modes of the 2-mer are tunable in real time in a laboratory with splittings as small

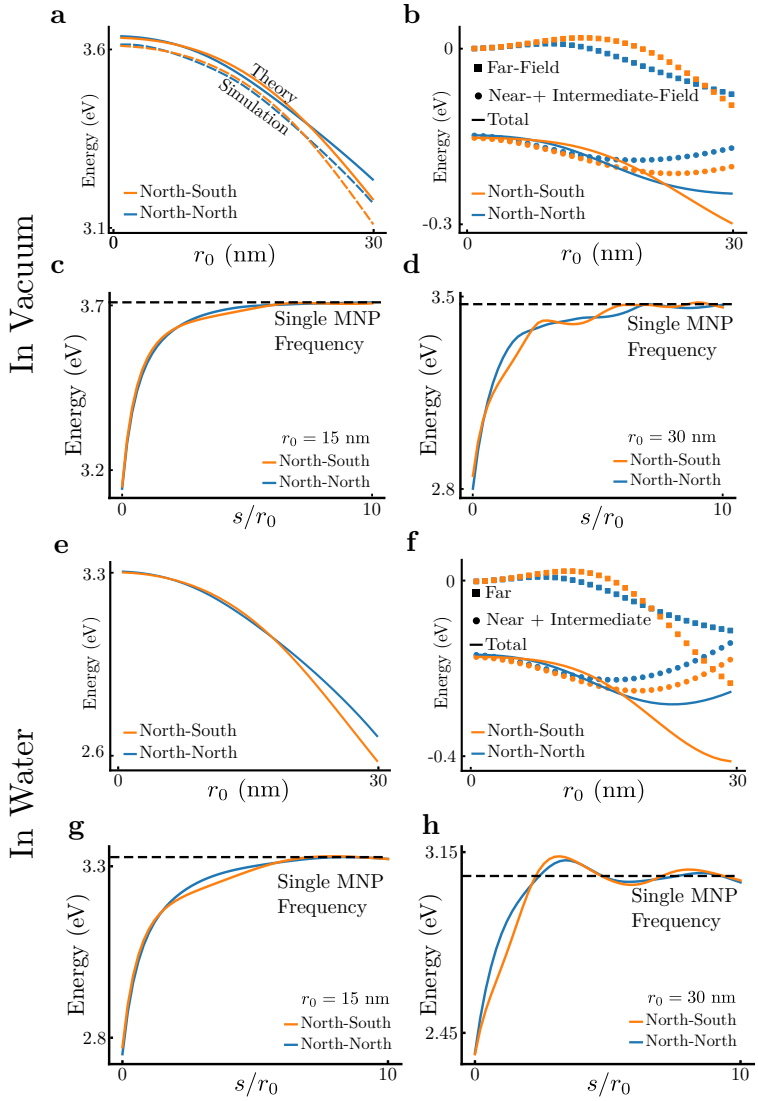

Figure 2: Eigenvalues and interaction energies as functions of total aggregate scale and interparticle distance for the magnetic modes of the 2mer. (a) The eigenvalues of the North-South (orange) and North-North (blue) modes for $r_0 = 1$ to 30 nm computed using the equations of motion (solid) and compared with full-wave simulations (dashed). Note the agreement to within 0.05 eV. The modes cross twice, once at around 7 nm and a second time at around 20 nm. (b) Total (solid), near- plus intermediate-field (circles), and far-field (squares) interaction energies for each mode as a function of increasing r_0. The splitting between the interaction energies in the far-field has the opposite sign as in the near- and intermeidate-field, resulting in the eigenmodes crossing. (c) and (d) Magnetic mode eigenvalues as a function of increasing interparticle distance, with $r_0 = 15$ and 30 nm, respectively. With increasing spacing, the eigenvalues tend towards the noninteracting, single-particle frequency and exhibit large oscillations and splittings. (e-h) Eigenvalues and interaction energies computed in a similar fashion to (a-d), with $\varepsilon_b = 1.77$, the dielectric constant of water.

as 0.01 eV and as large as 0.1 eV.

While the mode crossing of the 2mer are intersting and unexpected, in most cases the splittings between the modes are smaller than the breadth of the peaks associated with them in both scattering spectra and EEL spectra. Additionally, magnetic oligomers exhibit many other electrically bright modes that are close in energy and broad, which tends to wash out most spectra. In order to make magnetic oligomers useful, either the modes must be made fewer and more narrow, or techniques must be found that can identify and utilize the modes regardless of breadth. One such method is the measurement of directional or angle-resolved scattering.

4 Directional Scattering in the 2-mer

It has been predicted and shown experimentally that single magnetic oligomers scatter light anisotropically when both their magnetic dipole and their electric dipole are excited by light.[12,17] This is evident from scattering spectra, but can also be shown by computing the differential scattering pattern,[35,36]

$$\frac{dP}{d\Omega} = \frac{c}{8\pi}\left[r^2\hat{\mathbf{n}} \cdot \sum_i \mathbf{E}_i \times \sum_j \mathbf{B}_j^*\right] \tag{4}$$

where $\hat{\mathbf{n}}$ is the unit vector pointing to the detector a distance $r >> \lambda$ away and $\mathbf{E}_i$ and $\mathbf{B}_j^*$ are the electric and conjugate magnetic fields of the interfering collective modes of the 2mer. From here, we perform full-wave simulations to compute scattering spectra and differential scattering patterns on the 2mer and 3mers.[37] According to the diagram in Figure 3a and b, the incident light is polarized to excite a magnetic moment through the rings (perpendicular to the plane of the cluster, or the so-called z-direction) and an electric moment along the 2-mer's short axis (the so-called y-direction). Using the far-fields of these dipole moments in Equation 4, the differential scattering becomes[38]

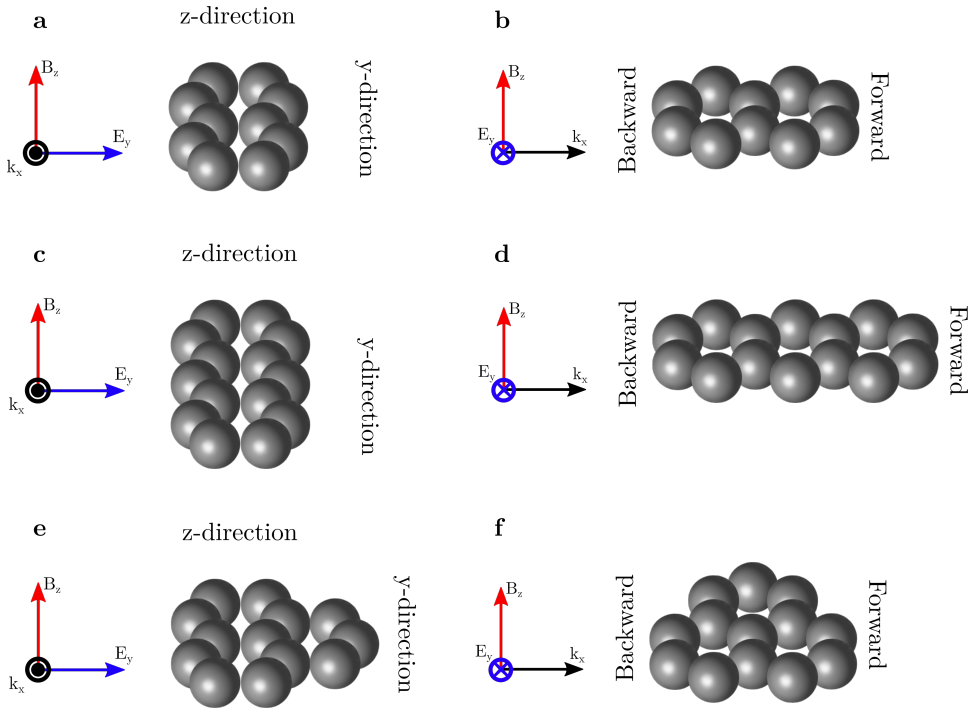

Figure 3: Diagrams of the incident light and orientation of the (a and b) 2mer, (c and d) linear 3mer, and (e and f) triangular 3mer systems to be referenced with Figures 4, 5, 7, and 8.

$$\frac{dP}{d\Omega} = \frac{ck^4N^2}{4\pi}\left[|\mathbf{d}_e|^2(1-(\hat{\mathbf{n}}\cdot\hat{\mathbf{y}})^2) + k^2R^2|\mathbf{d}_m|^2(1-(\hat{\mathbf{n}}\cdot\hat{\mathbf{z}})^2) + kR(\mathbf{d}_e\cdot\mathbf{d}_m^* + \mathbf{d}_e^*\cdot\mathbf{d}_m)(\hat{\mathbf{n}}\cdot\hat{\mathbf{x}})\right]. \tag{5}$$

Here, N is the number of particles in an aggregate, $\mathbf{d}_e$ is the individual electric dipole moment in the collective electric mode, $\mathbf{d}_m$ is the individual electric dipole moment in the collective magnetic mode, and R is the radius of a cluster. This equation can impart very powerful intuition and explains the optical scattering results very well. In the case that $d_m = 0$, the second and third terms vanish leaving only the first term which scatters in the pattern traditionally associated with a dipole. When $d_e = 0$, the first and third terms vanish, and the same pattern is recovered but in a different orientation. Finally, when both sets of dipole moments are non-zero, the third term contributes an overall asymmetry in the x-direction, which here is the light propagation direction. What this means is that when the collective

electric mode is excited, it should radiate; when the collective magentic mode is excited, it should radiate; when both are excited, they should interfere. Because of its simplicity, we use this model only to verify that the simulation results on the 2mer are consistent with intuition.

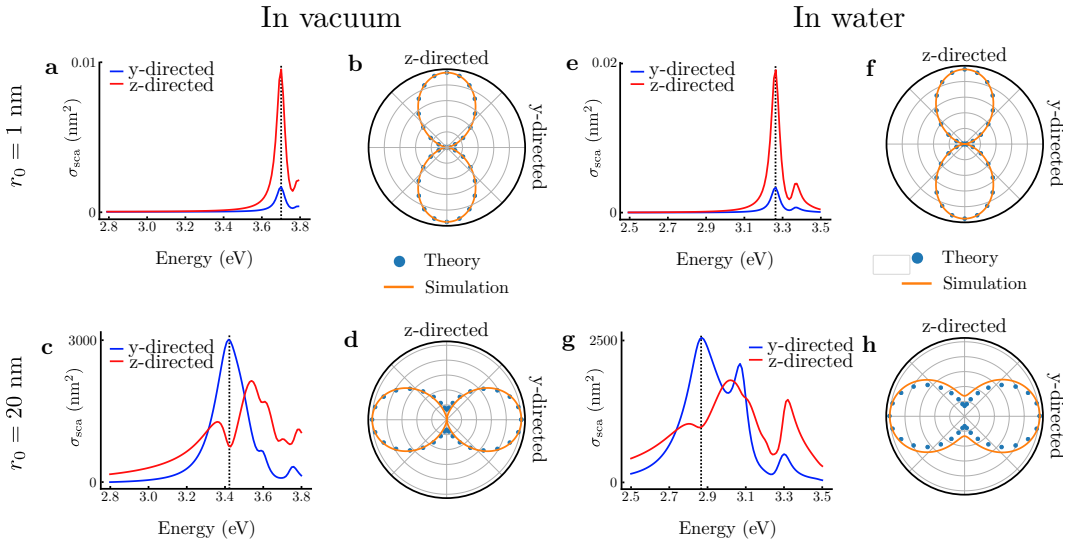

Figure 4: Scattering spectra and differential scattering patterns for the 2mer in vacuum and in water. (a) Scattering spectrum for the 2mer with $r_0 = 1$ nm and $s = 1$ displaying z-directed (red) and y-directed (blue) scattering. (b) Differential scattering pattern verifying that the z-directed scattering is much larger than the y-directed scattering. (c) Scattering spectrum for the 2mer with $r_0 = 20$ nm and $s = 1$, again with z-directed (red) and y-directed (blue) light. (d) Differential scattering pattern veryifying that at the chosen frequency, the y-directed scattering is greater than the z-directed scattering. (e-h) Scattering calculations in the same fashion as (a-d), with $\varepsilon_b = 1.77$, the dielectric constant of water.

Analyzing first the y- and z-oriented scattering gives a measure of the relative strength of the electric and magnetic modes. When $d_e >> d_m$ the y-directed scattering should appraoch zero while the z-oriented scattering will be maximized. This can be seen quite clearly in Figure 4a and b, where the electric dipole mode's dominance is evident through the primarily z-oriented scattering, especially at the peak frequency (dashed black line). As discussed previously, when the oligomers are small they behave quasistatically with almost no magnetic effects, so it is expected that the purely electric physics should dominate. Figure **??**c and d shows that at larger sizes the dominance of either y- or z-directed scattering is frequency dependent, signifying that the magnetic dipole moment can dominate the scattered light at

certain frequencies. The scattering pattern in (d) corresponds to the black dashed line in (c), emphasizing the frequency at which the magnetic dipole is strongest compared to the electric dipoles. This shows that different colors of light are scattered in different directions, which is in part suggested by the R-dependence encoded into the scattering pattern, but also depends on the oscillator strength of the entire mode. At the resonant frequency of the magnetic mode, it dominates the scattering pattern, but at other frequencies the electric dipole modes dominate. This suggests that the magnetic mode is much narrower and harder to force than the electric modes. This is interesting because this implies a method of detecting the frequency at which the all-North magnetic mode significantly impacts the optical properties of a given magnetic oligomer. Further emphasizing this is the fact that changing the aggregation scheme while probing at the same frequency shifts the radiation pattern back towards that of the electrically dominated system, as depicted in [**Figure not done yet!**]. Moving the 20 nm radius particles farther apart shifts the resonant frequency of the magnetic mode of the 2mer, so looking at the same frequncy as before yields a different scattering pattern. This offers a way to controllably choose the directionality of specific colors of light by manipulating the aggregation scheme of magnetic oligomers. These results are consistent in water as well, as shown in Figure **??**e-h.

Using the y- and z-directed scattering to understand the relative strength of the magnetic and electric dipole moments is only one side of the story. Looking instead at the x- and z-directed scattering opens up a tool to quantify the extent to which electric and magnetic plasmons interfere with one another. As suggested by the third term of Equation 5, in the direction of propagation we should expect to see asymmetry when both the electric dipole moment and magnetic dipole moment are of appreciable magnitude. Figure 5 shows spectra computed in the forward and backward direction for particles of $r_0 = 1$ nm and 20 nm (a and c) as well as differential scattering patterns in the xz-plane (b and d) in vacuum, and similarly in water (e-h). The differential scattering patterns have been computed at the frequencies that maximize the forward-to-backward ratio. As suggested by the R-dependence and the

dependence on dipole strength in Equation 5, at small sizes the radiation is isotropic in the forward (red) and backward (blue) direction. This again makes sense, as small oligomers are dominated by electric near-field effects. However, with increasing size, the interference term in Equation 5 begins to influence the spectrum and the scattering, leading to a large amount of directional radiation. Like before, this is dependent upon not only the size of the system but upon the oscillator strength of each mode, and so probing off resonance of the magnetic mode diminshes its influence and leads to more significant backward-directed radiation. However, at all frequencies the forward scattering is larger than the backward scattering, and even upon changing the interparticle distance this remains true. This suggests that once the magnetic mode is strong and broad enough to interfere with the electric modes, the directional radiation can not be completely turned off except by moving the particles infinitely far away from each other. Furthermore, this absolutely must be a collective effect as the constituent particles here are too small to radiate unidirectionally by themselves. Magnetic dipole-electric dipole scattering interference has been predicted and observed in metal-dielectric core-shell systems and single magnetic oligomer systems, and directional or angle-resolved scattering experiments are entirely possible on metal nanoparticle aggregates.[12,39–42]

5 Eigenvalue Calculations on the 3mers

The model presented earlier in this paper can also be applied to the 3mer systems. Looking first at Figure 1, each 3mer supports three magnetic modes, rather than two. However, the triangular 3mer's two electric dipole modes (f and g) are degenerate. This is represented in Figure 6, where the plots concerning the linear 3mer have 3 traces and the plots concerning the triangular 3mer have two traces. What is interesting about this analysis is that the 3mers do not differ greatly in spectral ordering from the 2mer. The eigenvalue plots and the interaction energy plots have similar qualitative features amongst all three systems. This

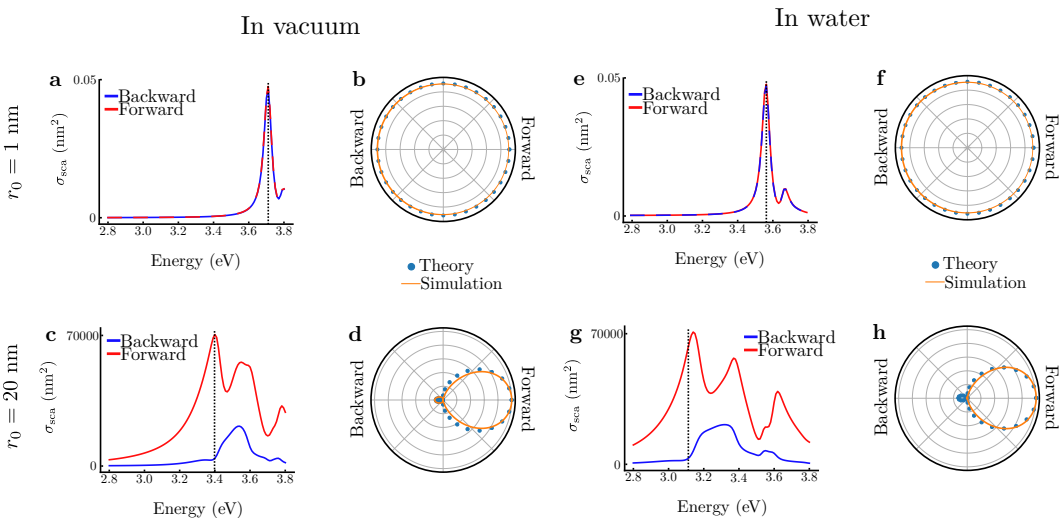

Figure 5: Forward and backward scattering spectra and differential scattering patterns for the 2mer. (a) Forward (red) and backward (blue) scattering spectra for the 2mer with $r_0 = 1$ nm and $s = 1$ nearly overlap. (b) The isotropic radiation pattern in the forward and backward direction computed using the model in Equation 5 (blue dots) and full-wave simulations (orange line). (c) Forward (red) and backward (blue) scattering spectra for the 2mer with $r_0 = 20$ nm and $s = 1$ are vastly different, showing that the forward scattering is almost always greater than the backward scattering. (d) The differential scattering pattern at the frequency marked by the dashed line in (c) shows that the scattering is nearly unidirectional both using the model (blue dots) and simulations (orange). (e-h) Scattering spectra and patterns computed in the same way as (a-d), except with $\varepsilon = 1.77$.

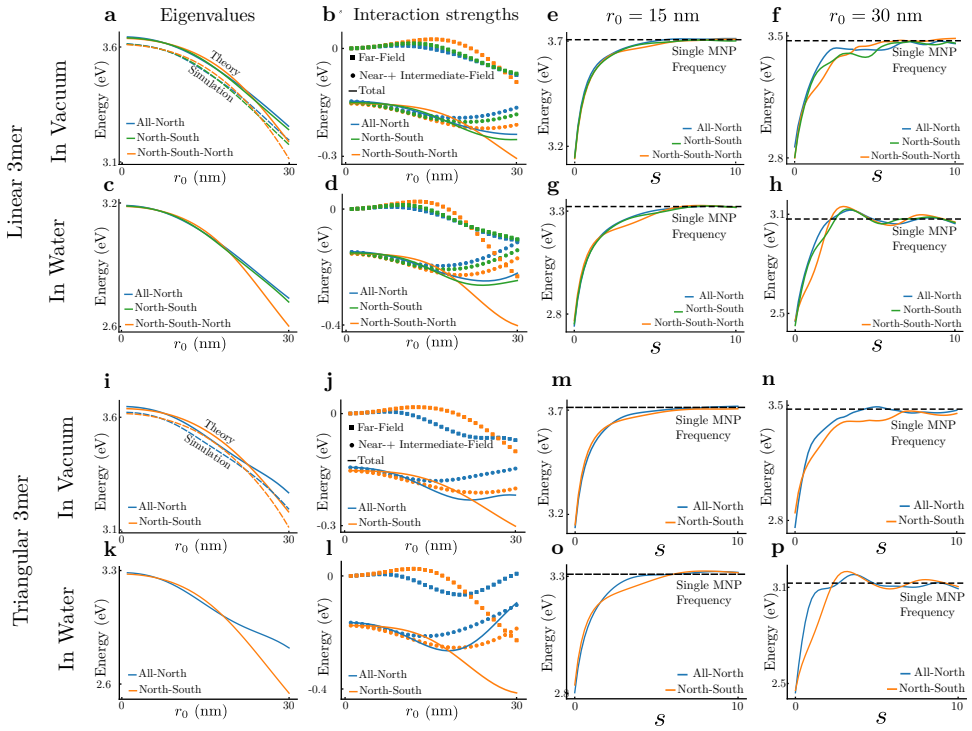

Figure 6: Eigenvalues and interaction energies of the magnetic modes of both the linear and triangular 3mers in vacuum and water. (a) The eigenvalues computed from the model on the three modes of the linear 3mer, showing crossing points at around 7.5 nm and 21 nm and compared with simulation results (dashed lines). (b) Interaction energies computed from Equation 3, with the far-field (squares) being entirely responsible for the crossing points in (a) while the near- and intermediate-field terms (circles) contribute only a net shift to the total (solid) interaction. (c and d) Similar plots to (a and b) with a background of water, which moves both crossing points to smaller size. (e) Eigenvalues as a function of interparticle spacing for particles of radius 15 nm, exhibit multiple crossings and low-amplitude oscillations when compared to larger (f) particles. (g and h) Similar results to (a and b), with a background of water, causing a net shift to lower energy of all eigenvalues and larger oscillations, but no drastic qualitative change. (i-p) Display similar results to (a-h) for the triangular 3mer. The analysis is very similar, as the eigenmodes have crossing points in similar locations and the eigenvalues and interaction energies are similarly impacted by the background of water.

may be evident of a kind of saturation length to individual electric plasmon interaction, predicted in previous work.[28] However, for the purposes of this paper, this simply shows that the model can be extended to larger systems without loss of accuracy or efficiency. More importantly, these magnetic modes can influence the directionality of scattered light, much like those of the 2mer.

6 Scattering Results from the 3mers

Now that we have thoroughly analyzed the properties of the 2mer, we next present results on the two 3mers mentioned previously, whose modes and aggregation schemes were displayed in Figure 1. Calculations similar to those presented in Figure 2 for the linear and triangular 3mers are shown in the Supporting Information. These results show no new trends, but verify that the theoretical method works for larger aggreagtes with more complicated aggregation schemes. From here, we present scattering spectra and differential scattering patterns for both 3mers.

Much like the 2mer, The directionality of scattered light is a measure of how much the magnetic dipoles of the 3mers contribute to their overall optical properties. Introducing a third ring at the end of the 2mer to produce the linear 3mer does not starkly change the optical properties, except that the dominance of the magnetic mode occurs at even smaller sizes, with $r_0 = 15$ nm, as opposed to 20 nm in the 2mer. The spectra and differential scattering patterns in Figure 7 share a strong resemblance to those of the 2mer, showing that at small sizes, the z-directed scattering dominates and the forward and backward scattering are isotropic. This is evidence that only a net electric diple moment is exciteable on small systems. At large size, the magnetic and electric dipole moments fight for dominance at different frequencies, but at all frequencies the forward scattering is much larger than the backward scattering.

The triangular 3mers exhibit new effects that can't be explained using either the 2mer or

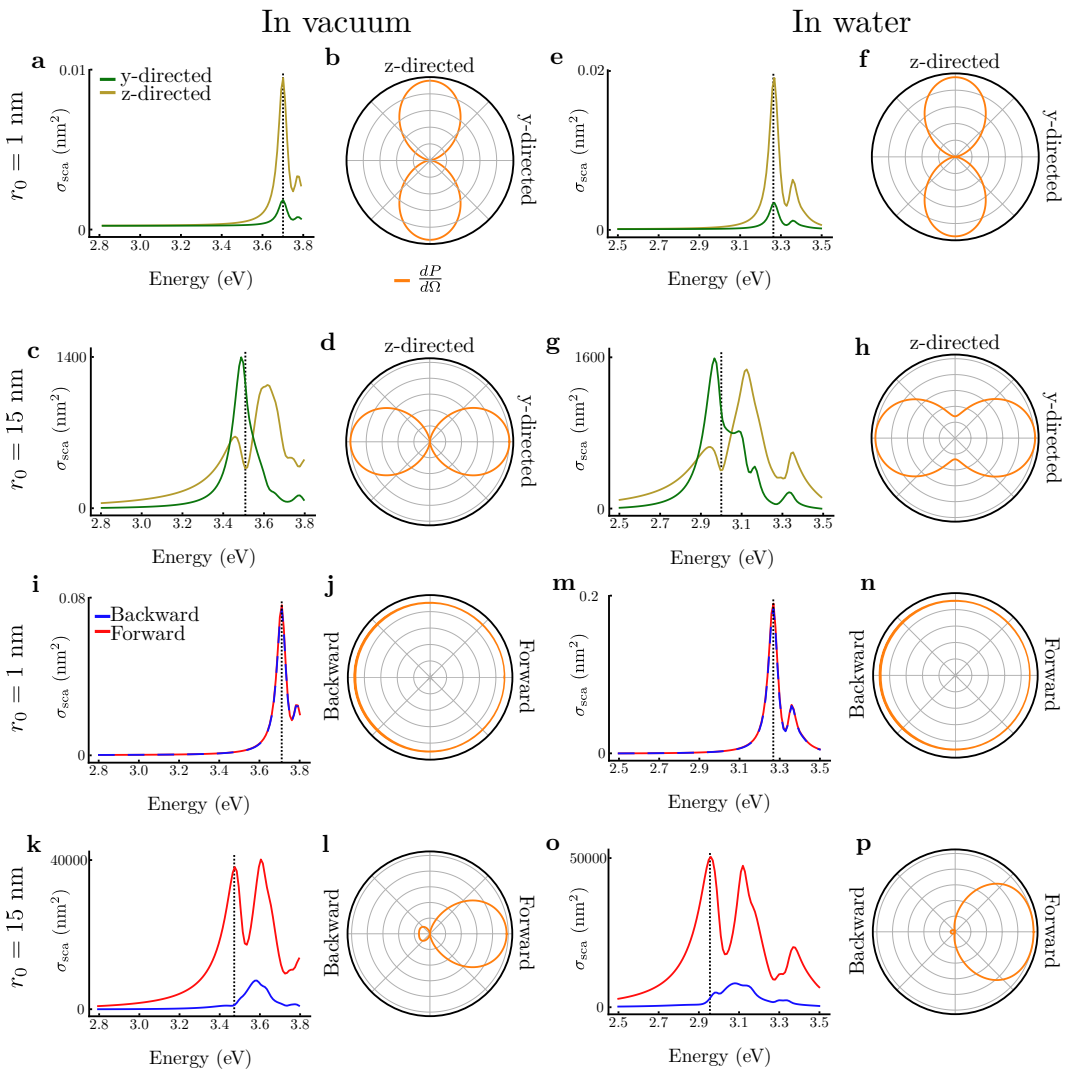

Figure 7: (a-h) Scattering spectra and differential scattering patterns comapring the y- (blue) and z-directed (red) scattering of the linear 3mer. (i-p) Forward (red) and backward (blue) scattering spectra and scattering patterns for the linear 3mer. (a) The y-directed scattering is much larger than the z-directed scattering for a linear 3mer with $r_0 = 1$ nm and $s = 1$, confirmed by (b) the simulated differential scattering in that plane. For a linear 3mer with $r_0 = 15$ nm (c), the difference between the two directions depends on frequency. At the frequency marked by the dotted line, the differential scattering pattern in (d) shows that the y-directed scattering is much higher than z-directed. (e-h) Similar computations as in (a-d), except performed with a background of water. (i) The forward and backward scattering for a linear 3mer with $r_0 = 1$ nm and $s = 1$ are nearly identical, as confirmed by (j) the isotropic scattering pattern. (k) For a 3mer of larger particles, the forward scattering is greater than the backward scattering at all computed frequencies. At the frequency marked by the dotted line, (l) the diffraction pattern shows a large degree of directionality. (m-p) Similar calculations as (i-l), computed in water.

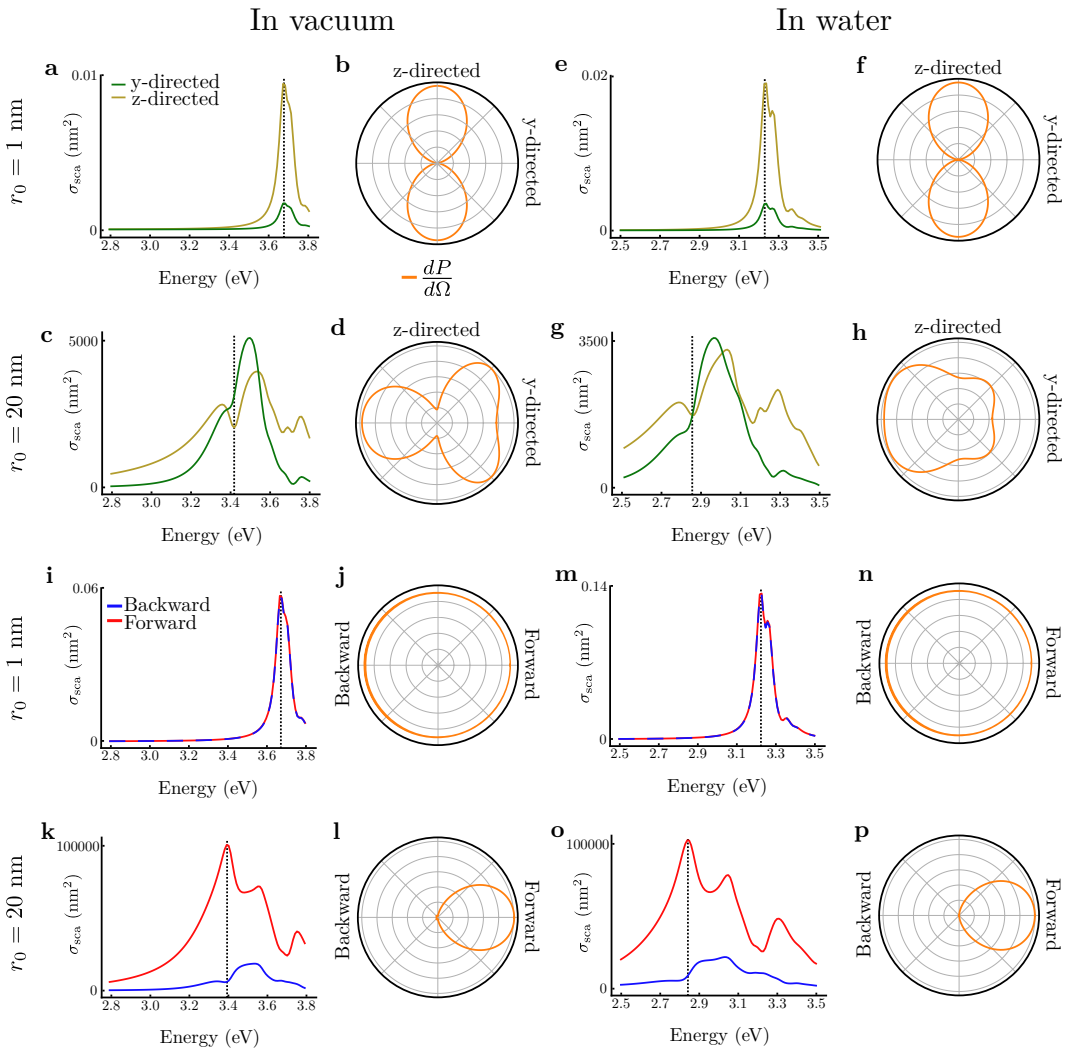

Figure 8: Scattering spectra and differential scattering patterns computed in the y- and z-directions (a-h) and in the forward and backward directions (i-p). (a) The z-directed scattering is far greater than the y-directed scattering for the triangular 3mer with $r_0 = 1$ nm and $s = 1$, owing to the excitation of only a net electric dipole moment in this size regime. This is confirmed by (b) the differential scattering pattern. (c) When the 3mer is composed of particles with $r_0 = 20$ nm, the directionality of light is frequency-dependent. Contrary to previous results, the peaks and dips in each scattering direction are uncorrelated, which is confirmed by (d) the differential scattering pattern collected at the frequency marked by the dashed line. This shows that some other collective mode of the system is weakly interfering and radiating, disrupting the symmetry expected from linear magnetic oligomers. These results are reproduced in water in (e-h). Similarly to the 2mer and the linear 3mer, (i) the forward (red) and backward (blue) scattering at small sizes are nearly equal, which is confirmed by (j) the differential scattering pattern. At larger sizes, (k and l) the triangular 3mer scatters light nearly completely unidirectionally at the chosen frequency, evidence of almost perfect interference between the magetic and electric dipole moments in the system. The results in water are qualitatively similar (m-p), showing that these properties do not drastically change in medium.

linear 3mer for comparison. Figure 8 shows that at small sizes, the triangular 3mer behaves much like the 2mer and the linear 3mer, likely because it fits entirely into a wavelength of light and is too small for magentic effects to matter. However, at large sizes, the spectra and scattering patterns of the triangular 3mer do not exhibit nicely correlated peaks and dips the way that the 2mer and linear 3mer do. This is likely because of the threefold symmetry of the triangular 3mer. Previous work has shown that systems with threefold symmetry exhibit unexpected directionality in their scattered radiation.[42] This is likely due to the degeneracy of the dipole moments on the this 3mer and the ability to weakly excite electric dipole moments with different orientations using only one polarization of light (imagine rotating Figure 1f about a threefold axis).

Scattering calculations on the linear 3mer show that preserving twofold symmetry, and keeping electric dipole moments with different orientations spectrally distinct, does not starkly change the optical properties of a magnetic oligomer but rather causes the magnetic effects to take over at smaller sizes. The opposite is true of the triangular 3mer, which shows that giving a magnetic oligomer system some kind of radial symmetry makes the distinction between electric dipole scattering and magnetic dipole scattering harder to determine. However, all of this points to unique and direct control over the directionality and color of scattered photons.

7 Conclusion

Using a simple tight-binding model, we have built in retardation effects in order to elucidate the spectral tunability of magnetic plasmon oligomers. The key to observing and using magnetic plasmons lies in the direction in which they scatter light. Planar magnetic oligomers constructed of fused rings of nanoparticles exhibit all the usual electric plasmon resonances, but also exhibit magnetic dipole moments oriented solely perpendicular to the plane of the oligomer. A properly polarized exciting field can probe simultaneously the in-plane

electric plasmons and the out-of-plane magnetic plasmons. As a result, the scattering spectra and patterns will exhibit signatures of magnetic dipole dominance and magnetic-electric interference. These properties make magnetic plasmon oligomers an ideal candidate for the direction-dependent manipulation of light.

Acknowledgement

CEI for money, HPC/Hyak/Mox for computing time, Niket and Harrison for good conversations.

References

(1) Karaveli, S.; Zia, R. Strong Enhancement of Magnetic Dipole Emission in a Multilevel Electronic System. *Opt. Lett.* **2010**, *35*, 3318–3320.

(2) Noginova, N.; Zhu, G.; Mavy, M.; Noginov, M. Magnetic Dipole Based Systems for Probing Optical Magnetism. *J. Appl. Phys.* **2008**, *103*, 07E901.

(3) Wang, J.; Fan, C.; He, J.; Ding, P.; Liang, E.; Xue, Q. Double Fano Resonances Due to Interplay of Electric and Magnetic Plasmon Modes in Planar Plasmonic Structure with High Sensing Sensitivity. *Opt. Express* **2013**, *21*, 2236–2244.

(4) Zhu, Z.; Bai, B.; You, O.; Li, Q.; Fan, S. Fano Resonance Boosted Cascaded Optical Field Enhancement in a Plasmonic Nanoparticle-in-Cavity Nanoantenna Array and its SERS Application. *Light: Science and Applications* **2015**, *4*, e296.

(5) Lee, K.-L.; Huang, J.-B.; Chang, J.-W.; Wu, S.-H.; Wei, P.-K. Ultrasensitive Biosensors Using Enhanced Fano Resonances in Capped Gold Nanoslit Arrays. *Scientific Reports* **2015**, *5*, 8547.

(6) Wu, C.; Khanikaev, A. B.; Adato, R.; Arju, N.; Yanik, A. A.; Altug, H.; Shvets, G. Fano-Resonant Asymmetric Metamaterials for Ultrasensitive Spectroscopy and Identification of Molecular Monolayers. *Nat. Mat.* **2012**, *11*, 69–75.

(7) Cetin, A. E.; Altug, H. Fano Resonant Ring/Disk Plasmonic Nanocavities on Conducting Substrates for Advanced Biosensing. *ACS Nano* **2012**, *6*, 9989–9995.

(8) Zhang, S.; Bao, K.; Halas, N. J.; Xu, H.; Nordlander, P. Substrate-Induced Fano Resonances of a Plasmonic Nanocube: a Route to Increased-Sensitivity Localized Surface Plasmon Resonance Sensors Revealed. *Nano Lett.* **2011**, *11*, 1657–1663.

(9) Liu, H.; Genov, D. A.; Wu, D. M.; Liu, Y. M.; Steele, J. M.; Sun, C.; Zhu, S. N.; Zhang, X. Magnetic Plasmon Propagation Along a Chain of Connected Subwavelength Resonators at Infrared Frequencies. *Phys. Rev. Lett.* **2006**, *97*, 243902.

(10) Liu, N.; Mukherjee, S.; Bao, K.; Brown, L. V.; Dorfmüller, J.; Nordlander, P.; Halas, N. J. Magnetic Plasmon Formation and Propagation in Artificial Aromatic Molecules. *Nano Lett.* **2011**, *12*, 364–369.

(11) Liu, N.; Mukherjee, S.; Bao, K.; Li, Y.; Brown, L. V.; Nordlander, P.; Halas, N. J. Manipulating Magnetic Plasmon Propagation in Metallic Nanocluster Networks. *ACS Nano* **2012**, *6*, 5482–5488.

(12) Sheikholeslami, S. N.; GarcÃŋa-Etxarri, A.; Dionne, J. A. Controlling the Interplay of Electric and Magnetic Modes via Fano-like Plasmon Resonances. *Nano Letters* **2011**, *11*, 3927–3934, PMID: 21819059.

(13) Scholl, J. A.; Garcia-Etxarri, A.; Aguirregabiria, G.; Esteban, R.; Narayan, T. C.; Koh, A. L.; Aizpurua, J.; Dionne, J. A. Evolution of Plasmonic Metamolecule Modes in the Quantum Tunneling Regime. *ACS Nano* **2016**, *10*, 1346–1354, PMID: 26639023.

(14) Weick, G.; Woollacott, C.; Barnes, W. L.; Hess, O.; Mariani, E. Dirac-like Plasmons in Honeycomb Lattices of Metallic Nanoparticles. *Phys. Rev. Lett.* **2013**, *110*, 106801.

(15) Greybush, N. J.; Liberal, I. n.; Malassis, L.; Kikkawa, J. M.; Engheta, N.; Murray, C. B.; Kagan, C. R. Plasmon Resonances in Self-Assembled Two-Dimensional Au Nanocrystal Metamolecules. *ACS Nano* **2017**, *11*, 2917–2927, PMID: 28190335.

(16) Cherqui, C.; Bigelow, N. W.; Vaschillo, A.; Goldwyn, H.; Masiello, D. J. Combined Tight-Binding and Numerical Electrodynamics Understanding of the STEM/EELS Magneto-Optical Responses of Aromatic Plasmon-Supporting Metal Oligomers. *ACS Photonics* **2014**, *1*, 1013–1024.

(17) Cherqui, C.; Wu, Y.; Li, G.; Quillin, S. C.; Busche, J. A.; Thakkar, N.; West, C. A.; Montoni, N. P.; Rack, P. D.; Camden, J. P. .; Masiello, D. J. STEM/EELS Imaging of Magnetic Hybridization in Symmetric and Symmetry-Broken Plasmon Oligomer Dimers and All-Magnetic Fano Interference. *Nano Lett.* **2016**, *16*, 6668–6676, PMID: 27673696.

(18) Purcell, E. M.; Pennypacker, C. R. Scattering and Absorption of Light by Nonspherical Dielectric Grains. *Astrophys. J.* **1973**, *186*, 705–714.

(19) Brandl, D. W.; Mirin, N. A.; Nordlander, P. Plasmon Modes of Nanosphere Trimers and Quadrumers. *J. Phys. Chem. B* **2006**, *110*, 12302–12310.

(20) Myroshnychenko, V.; Rodriguez-Fernandez, J.; Pastoriza-Santos, I.; Funston, A. M.; Novo, C.; Mulvaney, P.; Liz-Marzan, L. M.; Garcia de Abajo, F. J. Modelling the optical response of gold nanoparticles. *Chem. Soc. Rev.* **2008**, *37*, 1792–1805.

(21) Turner, M. D.; Hossain, M. M.; Gu, M. The Effects of Retardation on Plasmon Hybridization within Metallic Nanostructures. *New J. of Phys.* **2010**, *12*, 083062.

(22) Dahmen, C.; Schmidt, B.; von Plessen, G. Radiation Damping in Metal Nanoparticle Pairs. *Nano Lett.* **2007**, *7*, 318–322, PMID: 17243751.

(23) Rechberger, W.; Hohenau, A.; Leitner, A.; Krenn, J.; Lamprecht, B.; Aussenegg, F. Optical Properties of Two Interacting Gold Nanoparticles. *Opt. Commun.* **2003**, *220*, 137 – 141.

(24) Kottmann, J. P.; Martin, O. J. F. Retardation-Induced plasmon Resonances in Coupled Nanoparticles. *Opt. Lett.* **2001**, 1096–1098.

(25) Haynes, C. L.; McFarland, A. D.; Zhao, L.; Van Duyne, R. P.; Schatz, G. C.; Gunnarsson, L.; Prikulis, J.; Kasemo, B.; Käll, M. Nanoparticle Optics: The Importance of Radiative Dipole Coupling in Two-Dimensional Nanoparticle Arrays. *J. Phys. Chem. B* **2003**, *107*, 7337–7342.

(26) Bouhelier, A.; Bachelot, R.; Im, J. S.; Wiederrecht, G. P.; Lerondel, G.; Kostcheev, S.; Royer, P. Electromagnetic Interactions in Plasmonic Nanoparticle Arrays. *J. Phys. Chem. B* **2005**, *109*, 3195–3198, PMID: 16851340.

(27) Kinnan, M. K.; Chumanov, G. Plasmon Coupling in Two-Dimensional Arrays of Silver Nanoparticles: II. Effect of the Particle Size and Interparticle Distance. *J. Phys. Chem. C* **2010**, *114*, 7496–7501.

(28) Near-, middle-, and far-field dipolar interactions in gold nanoparticle arrays. 2016; pp 97240B–97240B–8.

(29) Cherqui, C.; Thakkar, N.; Li, G.; Camden, J. P.; Masiello, D. J. Characterizing Localized Surface Plasmons Using Electron Energy-Loss Spectroscopy. *Annual Review of Physical Chemistry* **2016**, *67*, 331–357, PMID: 27215817.

(30) Jain, P. K.; El-Sayed, M. A. Noble Metal Nanoparticle Pairs: Effect of Medium for Enhanced Nanosensing. *Nano Letters* **2008**, *8*, 4347–4352, PMID: 18956905.

(31) Yang, A.; Hryn, A. J.; Bourgeois, M. R.; Lee, W.-K.; Hu, J.; Schatz, G. C.; Odom, T. W. Programmable and reversible plasmon mode engineering. *P. Natl. Acad. Sci.* **2016**, *113*, 14201–14206.

(32) Qian, Z.; Guye, K. N.; Masiello, D. J.; Ginger, D. S. Dynamic Optical Switching of Polymer/Plasmonic Nanoparticle Hybrids with Sparse Loading. *J. Phys. Chem. B* **2017**, *121*, 1092–1099, PMID: 28075134.

(33) Kuzyk, A.; Urban, M. J.; Idili, A.; Ricci, F.; Liu, N. Selective control of reconfigurable chiral plasmonic metamolecules. *Sci. Adv.* **2017**, *3*.

(34) Cheng, W.; Campolongo, M. J.; Cha, J. J.; Tan, S. J.; Umbach, C. C.; Muller, D. A.; Luo, D. Free-standing nanoparticle superlattice sheets controlled by DNA. *Nat. Mat.* **2009**, *8*, 519–525.

(35) Jackson, J. D. *Classical Electrodynamics*, 3rd ed.; Wiley: New York, NY, 1999.

(36) Schwinger, J.; Deraad, L.; Milton, K.; Tsai, W.; Norton, J. *Classical Electrodynamics*; Advanced book program; Avalon Publishing, 1998.

(37) Hohenester, U.; Trügler, A. MNPBEM - A Matlab Toolbox for the Simulation of Plasmonic Nanoparticles. *Comp. Phys. Comm.* **2012**, *183*, 370 – 381.

(38) Alù, A.; Salandrino, A.; Engheta, N. Negative effective permeability and left-handed materials at optical frequencies. *Opt. Express* **2006**, *14*, 1557–1567.

(39) Liu, W.; Miroshnichenko, A. E.; Neshev, D. N.; Kivshar, Y. S. Broadband Unidirectional Scattering by Magneto-Electric CoreâĂŞShell Nanoparticles. *ACS Nano* **2012**, *6*, 5489–5497, PMID: 22545872.

(40) Coenen, T.; Bernal Arango, F.; Femius Koenderink, A.; Polman, A. Directional emission from a single plasmonic scatterer. *Nat. Comm.* **2014**, *5*, 3250.

(41) Powell, A. W.; Hjerrild, N.; Watt, A. A. R.; Assender, H. E.; Smith, J. M. Directional plasmonic scattering from metal nanoparticles in thin-film environments. *Appl. Phys. Lett.* **2014**, *104*, 081110.

(42) Tanaka, Y. Y.; Shimura, T. Tridirectional Polarization Routing of Light by a Single Triangular Plasmonic Nanoparticle. *Nano Lett.* **2017**, *17*, 3165–3170, PMID: 28388075.

Graphical TOC Entry

Some journals require a graphical entry for the Table of Contents. This should be laid out "print ready" so that the sizing of the text is correct.
Inside the `tocentry` environment, the font used is Helvetica 8 pt, as required by *Journal of the American Chemical Society*.
The surrounding frame is 9 cm by 3.5 cm, which is the maximum permitted for *Journal of the American Chemical Society* graphical table of content entries. The box will not resize if the content is too big: instead it will overflow the edge of the box.
This box and the associated title will always be printed on a separate page at the end of the document.